Archives of Materials Science and Engineering

Volume 109
Issue 2
June 2021
Pages 65-79

International Scientific Journal
published monthly by the
World Academy of Materials
and Manufacturing Engineering

DOI: 10.5604/01.3001.0015.2625

Effects of yttria content and sintering temperature on the microstructure and tendency to brittle fracture of yttria-stabilized zirconia

V.V. Kulyk [a,*], Z.A. Duriagina [a,b], B.D. Vasyliv [c], V.I. Vavrukh [a], P.Ya. Lyutyy [a], T.M. Kovbasiuk [a], M.Ya. Holovchuk [c]

[a] Lviv Polytechnic National University, 12 Bandera St., Lviv, 79013, Ukraine
[b] The John Paul II Catholic University of Lublin, Al. Racławickie 14, 20-950 Lublin, Poland
[c] Karpenko Physico-Mechanical Institute of the National Academy of Sciences of Ukraine, 5 Naukova St., Lviv, 79060, Ukraine
* Corresponding e-mail address: kulykvolodymyrvolodymyrovych@gmail.com
ORCID identifier: https://orcid.org/0000-0001-5999-3551 (V.V.K.);
https://orcid.org/0000-0002-2585-3849 (Z.A.D.); https://orcid.org/0000-0002-8827-0747 (B.D.V.);
https://orcid.org/0000-0002-3143-2522 (V.I.V.); https://orcid.org/0000-0001-7266-1113 (P.Ya.L.);
https://orcid.org/0000-0003-2792-0555 (T.M.K.)

ABSTRACT

Purpose: The purpose of this work is to evaluate the propensity to brittle fracture of YSZ ceramics stabilized by the various amount of yttria, based on a study of changes in the microstructure, phase composition, and fracture micromechanisms.

Design/methodology/approach: The series of 3YSZ, 4YSZ, and 5YSZ ceramic specimens were sintered in an argon atmosphere. Three sintering temperatures were used for each series: 1450°C, 1500°C, and 1550°C. Microhardness measurements were performed on a NOVOTEST TC-MKB1 microhardness tester. The configuration of the imprints and cracks formed was studied on an optical microscope Neophot-21. The fracture toughness of the material was estimated using both the Vickers indentation method and a single-edge notch beam (SENB) test performed under three-point bending at 20°C in air. The microstructure and morphology of the fracture surface of the specimens were studied using a scanning electron microscope Carl Zeiss EVO-40XVP. The chemical composition was determined using an INCA ENERGY 350 spectrometer.

Findings: Peculiarities of changes in the microstructure, the morphology of specimens fracture surface, and mechanical characteristics of YSZ ceramic materials of different chemical and phase compositions sintered in a temperature range of 1450°C to 1550°C are found.

Research limitations/implications: To study the actual behaviour of YSZ ceramic materials under operating conditions, it is necessary to evaluate their Young's moduli, strength, microhardness, and fracture toughness in an operating environment of the corresponding parameters (temperature, pressure, etc.).

Practical implications: Based on the developed approach to estimating the propensity to brittle fracture of the formed YSZ ceramic microstructure, it is possible to obtain YSZ ceramic material that will provide the necessary physical and mechanical properties of a wide variety of precision ceramic products.

Originality/value: An approach to estimating the propensity to brittle fracture of YSZ ceramics stabilized by the various amount of yttria is proposed based on two methods of evaluating crack growth resistance of materials, namely, the Vickers indentation method and SENB method.

Keywords: YSZ ceramics, Microhardness, Fracture toughness, Microstructure, Fracture micromechanism

Reference to this paper should be given in the following way:

V.V. Kulyk, Z.A. Duriagina, B.D. Vasyliv, V.I. Vavrukh, P.Ya. Lyutyy, T.M. Kovbasiuk, M.Ya. Holovchuk, Effects of yttria content and sintering temperature on the microstructure and tendency to brittle fracture of yttria-stabilized zirconia, Archives of Materials Science and Engineering 109/2 (2021) 65-79. DOI: https://doi.org/10.5604/01.3001.0015.2625

PROPERTIES

1. Introduction

Nowadays, many advanced ceramics enterprises can produce a wide variety of precision ceramic products customized to the clients' needs, ensuring a long life cycle for the products. Depending on the qualities required, the products are manufactured of sintered silicon carbide, aluminium oxide, partially stabilized zirconia, or other ceramics [1-6].

Ceramic products manufactured of yttria-stabilized zirconia (YSZ) are operated in high-temperature, high pressure, corrosive, and abrasion environments (petro-chemical industry), grinding, high-temperature, and high-speed conditions (textile, water hardware), high-pressure and high-temperature insulation conditions (other industries). According to the clients' needs and corresponding qualities required, the products are to be wear and corrosion resistant, thermal shock resistant, highly insulated, and possess high strength and air impermeability.

A conventional YSZ production process comprises the following stages: material acquisition (raw materials), material allocation, spray granulation, formation, sintering, grinding, product inspection, and packaging inspection. There are still issues on the structural integrity and lifetime of manufactured ceramic products which operate under the above-mentioned conditions [7-13]. Among them, the choice of chemical composition and manufacturing modes of material are the crucial ones that affect the resulting phase balance and physical and mechanical properties of the manufactured material [14-20].

In the works [21,22], based on studies of the phase evolution in plasma-sprayed YSZ coatings during annealing using XRD analysis and neutron scattering studies, it was found that metastable tetragonal YSZ decomposes into monoclinic and cubic phases as the yttria content in the tetragonal phase decreases. In the works [23,24], based on XRD studies on plasma-sprayed coatings and EB-PVD coatings, it was found that between 1300°C and 1400°C, the metastable tetragonal phase decomposes into a tetragonal phase with low yttria content and a cubic or tetragonal phase with high yttria content. In the work [25], XRD analysis was performed in combination with a transmission electron microscopy (TEM) study on EB-PVD coatings heat-treated at temperatures from 1100°C to 1500°C, and it was found that the metastable tetragonal YSZ phase decomposes into a tetragonal phase with low yttria content and both tetragonal and cubic phases with high yttria content. Alternation of layers with high and low yttria content was found in TEM images. Based on these results, using computer simulations, it was concluded that the domain boundaries have a cubic-like structure with a relatively high content of yttrium ions [26,27].

The authors of the work [28], based on studies of 2Y-TZP ceramics from powder obtained by detonation synthesis, found an unusual combination of both very high strength and fracture toughness without any correlation with grain size. Based on the revealed broad transformation zone with secondary microcracks and shear bands on the tensile side during bending of the specimens, it is assumed that this character of the fracture is responsible for the high fracture toughness. Similarly, in the work [29], based on the study of a series of specimens sintered at 1000°C for 10 h from pure zirconium dioxide powder and YSZ powder, phase transformations due to doping were revealed, which allowed understanding the structural properties of zirconia with and without doping for technological purposes.

In the work [30], the effect of Fe_2O_3 additives on the microstructure, mechanical properties, and translucency of zirconia with 3 mol% or 5 mol% Y_2O_3 was evaluated. The density, phase composition, roughness, microstructure, strength, and translucency of specimens sintered at 1475, 1500, 1550, and 1600°C for 2 h were analysed. After sintering at 1600°C, only tetragonal ZrO_2 was detected in specimens with 3% Y_2O_3, while in specimens with 5% Y_2O_3 the cubic ZrO_2 phase was detected. For specimens sintered at 1600°C, a significant increase in grain size (from 0.8 μm to 2.3 μm) with an increase in the Y_2O_3 content from 3% to 5% was revealed. The change in Fe_2O_3 content did not promote changes in the density, microstructure, or mechanical properties. However, the effect of the Y_2O_3 content on strength of the material was found.

The authors of the work [31] studied the resistance to low-temperature degradation of zirconium dioxide stabilized with 3 mol% Y_2O_3 (3Y-TZP), which additionally contained 0.25% Al_2O_3, as a material of monolithic restorations in dentistry. Such a phenomenon occurs when Y_2O_3-containing t-ZrO_2 is converted to m-ZrO_2 during aging at temperatures of 100-300°C. This conversion is accelerated in the presence of moisture and is followed by the degradation of the mechanical properties of the material. Taking into account the effect of pretreatment temperature on the biaxial strength of indented specimens, it is assumed that the durability of restorations will not lower if aged restorations retain residual compressive stresses on the surface corresponding to t→m phase transformation less than 52% in the environment. In the work [32], the lattice distortion after phase transformation was calculated using the Kikuchi-band based method, and the BSD results were compared with the results of XRD analysis.

The strength and wear resistance of materials of which products of the petrochemical and textile industries (bearings, mechanical seals bearings, friction slices, valve plates, ball valves, pipeline lining, nozzles, moulds, thermocouple protection tubes, etc.) are made, are traditionally the main property, according to which their bearing capacity is evaluated [31,33,34]. However, one of the key functional requirements for such products is high chemical inertness to avoid the interaction of the product material with operating environments [35-37]. Therefore, it is necessary to form an appropriate microstructure of the material of products, which would prevent its degradation at the boundary "environment-material" and the degradation of bulk material [38-45]. Due to such requirements for the microstructure of the material, strength may be an insufficient characteristic of its bearing capacity. There are more structurally sensitive methods for diagnosing the load-bearing capacity of ceramic materials and products, among which the indentation method is one of the most common mechanical methods [31,46-48]. In addition to this method, traditional fracture toughness tests with a variety of specimen shapes and loading schemes are used in fracture mechanics [30,33,35,36,46,47,49,50]. Therefore, it is advisable to study the mechanical behaviour of YSZ ceramic material, sintered in different modes, in particular, to investigate the relationship between its microstructure and the tendency to brittle fracture.

The work is aimed at evaluating the propensity to brittle fracture of YSZ ceramic material stabilized by the various amount of yttria, based on a study of changes in the microstructure, phase composition, and fracture micro-mechanisms.

2. Experimental procedures

In this work, commercial starting powders of ZrO_2 ceramics partially stabilized with 3, 4, and 5 mol% Y_2O_3 (hereinafter: 3YSZ, 4YSZ, and 5YSZ) from the Vol'nogorskii Mining and Smelting Plant, Ukraine have been studied. ZrO_2 starting powders with initial particle sizes of 100-150 nm and Y_2O_3 powders with initial particle sizes of 10-30 nm were used. Powders in corresponding ratios were thoroughly mixed in a drum mill with the presence of isopropyl alcohol. In addition to the mixture of ZrO_2 and Y_2O_3 powders, the slurry contained the following components: ethylcellulose (polymer bond), dibutyl phthalate (plasticizer), and isopropyl alcohol (solvent). To remove residual liquid from the powders after mixing, they were dried in an oven at 120°C until the loss of their weight was stopped. The powders were then calcined at 700°C to get a specific particle size distribution and phase composition. To improve compaction, 5 wt.% polyvinyl butyral (5% alcohol solution) was added to the prepared powders [51-54]. Series of prismatic specimens 4×4×50 mm in size were formed by the method of bilateral compaction in a metal mould under a pressure of 50 MPa. The specimens were then sintered in an electrical resistance furnace for 2 h in argon using a conventional sintering technique. Three sintering temperatures were used for each series: 1450°C, 1500°C, and 1550°C. In such a way, nine variants of material were obtained (Tab. 1).

This made it possible to investigate the effects of sintering temperature on the phase balance of the material as well as particle size distribution. After sintering, the side surfaces of all specimens were ground and polished to reach the required surface quality. The final size of each specimen was 3.5×3.5×50 mm.

Table 1.
Chemical composition and sintering modes of variants of the investigated material

Variant	Content of Y_2O_3, mol%	Sintering mode	
		Temperature, °C	Time, h
3YSZ-1450	3	1450	2
3YSZ-1500	3	1500	2
3YSZ-1550	3	1550	2
4YSZ-1450	4	1450	2
4YSZ-1500	4	1500	2
4YSZ-1550	4	1550	2
5YSZ-1450	5	1450	2
5YSZ-1500	5	1500	2
5YSZ-1550	5	1550	2

The microhardness of the investigated material variants was measured using a NOVOTEST TC-MKB1 microhardness tester under the indentation loads of 0.49 N, 0.98 N, 1.96 N, 2.94 N, 4.91 N, and 9.81 N.

Conditions for measuring the microhardness of materials are regulated by the relevant standards [55,56]. According to ASTM C 1327 [56], Vickers microhardness (in GPa) is calculated by the formula:

$$HV = 0.0018544\left(\frac{P}{d^2}\right) \quad (1)$$

where P is the indentation load (N) and d is the average length of the diagonals of the indentation imprint (mm).

Based on the values of the optically measured imprint diagonals, the microhardness tester automatically calculates the arithmetic mean value of the imprint diagonal length. After that, the value of microhardness is automatically calculated as the ratio of the load applied to the indenter to the inclined surface area of the imprint.

The microhardness of each material variant (Tab. 1) was determined by making at least 10 indentations for each of the selected load levels at 20°C in air.

The fracture toughness, which is estimated by calculating the critical stress intensity factor (SIF) K_{Ic}, is an important characteristic of the mechanical behaviour of metallic and ceramic materials, which allows assessing their propensity to brittle fracture due to the formation and growth of cracks [57-62]. A wide range of methods for estimating the fracture toughness of materials under Vickers pyramid indentation [63-76], each of which is thoroughly described and confirmed by analytical calculations and experiments, testifies to the universality of this approach. The formulas presented in these works contain both physical and mechanical parameters, as well as empirical coefficients, and this, accordingly, narrows the range of materials to the diagnosis of which these formulas can be applied. In the work [77], the K_{Ic} values were calculated for ZrO_2-Y_2O_3 ceramics according to each of the formulas proposed in the works [63-76], and these values were then compared with those obtained for such material by traditional methods of fracture mechanics. These studies allowed substantiating for the characterization of this material the following formula [73] as an optimal one:

$$K_{Ic} = 0.016\left(\frac{E}{H}\right)^{1/2}\left(\frac{P}{c^{3/2}}\right) \quad (2)$$

where E is Young's modulus (GPa), H is microhardness (GPa), P is the indentation load (N), and c is the radial crack length (m). To obtain the value of K_{Ic} in MPa·m$^{1/2}$, you need to multiply the value obtained by this formula by 10^{-6}.

Thus, this formula uses a set of power (Young's modulus of material, microhardness, and indentation load) and geometric (total crack length c according to ASTM C 1327 [56]) parameters.

Based on the results of these studies, in our work, we used the above-mentioned formula to assess the fracture toughness of the studied material variants.

Along with fracture toughness test by the Vickers indentation method, we used in this work a single-edge notch beam test under three-point bending [78-80]. An edge notch 0.1 mm in width was machined in a beam specimen using a diamond disk. The supporting roller span of the loading device was 14 mm. The tests were performed on the MTS Criterion E43.104 test machine at 20°C in air. The corresponding formulas [78-80] were used for calculating the critical SIF K_{Ic} of material. Five samples of each of the investigated material variants were tested and the average K_{Ic} value was calculated.

A scanning electron microscope (SEM) Carl Zeiss EVO-40XVP was used for studying microstructure and fracture surface morphology of specimens. To determine the chemical composition of the material in local areas, INCA ENERGY 350 spectrometer with an energy dispersive X-ray microanalysis was used. To study the geometry of imprints and cracks, an optical microscope Neophot-21 was used.

3. Results and discussion

3.1. Phase balance in the investigated YSZ ceramics

The obtained XRD patterns of the studied material variants exhibit, in general, the phase balance for 3YSZ, 4YSZ, and 5YSZ ceramics and the changes in the phase balance with changes in the sintering temperature from 1450°C to 1550°C.

Based on the analysis of XRD patterns, the competing effect of two different factors on the phase balance in the studied material variants was noticed. The sintering temperature of ceramics is one factor, and the content of the stabilizing Y_2O_3 additive is another one. In 3YSZ ceramics, the amount of tetragonal phase of zirconia increases with increasing sintering temperature from 1450°C to 1500°C, while the amount of monoclinic phase increases slightly, so no noticeable decrease in cubic phase is observed (Fig. 1a). However, with a further increase in the sintering temperature to 1550°C, despite maintaining the rate of increasing the tetragonal phase percentage, the amount of monoclinic phase increases very steeply and, accordingly, the amount of cubic phase decreases to about 2 wt.%.

Analysis of the phase balance in 5YSZ ceramics showed that with increasing sintering temperature from 1450°C to 1500°C the amount of tetragonal phase of zirconia, in contrast to 3YSZ ceramics, decreases rapidly, while the amount of monoclinic phase increases and the percentage of cubic phase (about 5 wt.%) does not change (Fig. 1c). With a further increase in the sintering temperature to 1550°C, the rate of decreasing the tetragonal phase percentage remains constant, and the amount of monoclinic phase no longer increases but rather decreases. This is probably a consequence of a sharp increase in the amount of cubic phase due to its stabilization at this temperature with a large enough amount of Y_2O_3.

The phase balance in 4YSZ ceramics, which is intermediate in terms of the stabilizing Y_2O_3 additive percentage, reflects the competing effect of the two above-mentioned factors, namely, the sintering temperature of the ceramics and the content of the stabilizing Y_2O_3 additive. As the sintering temperature increases from 1450°C to 1500°C, the amount of tetragonal phase of zirconia decreases rapidly, while the amount of monoclinic phase increases slightly and the amount of cubic phase increases significantly (Fig. 1b). This tendency to change the phase balance in the material is the opposite of the trend found in 3YSZ ceramics and is probably the result of a higher content of the stabilizing Y_2O_3 additive. However, we see in the graph (Fig. 1b) that such an advantage in the stabilizing additive is insufficient to stabilize the cubic phase at higher sintering temperatures. Therefore, with a further increase in the sintering temperature to 1550°C, the stabilizing additive provides only an increased amount of tetragonal phase of zirconia. The rate of increasing the monoclinic phase percentage remains constant, and the amount of cubic phase decreases to about 2.5 wt.%.

The XRD patterns of the material given for the selected modes (Fig. 2, variants 3YSZ-1550, 4YSZ-1500, 5YSZ-1450, and 5YSZ-1550) reflect in detail the above-mentioned regularities of the phase balance of the studied material compositions.

The XRD pattern of 3YSZ ceramics of variant 3YSZ-1550 contains peaks of the t-ZrO_2, c-ZrO_2, and m-ZrO_2 phases (Fig. 2a). However, the peaks of the c-ZrO_2 phase are very low, which corresponds to the amount of this phase of about 2 wt.% (Fig. 1a), whereas the t-ZrO_2 phase peaks are relatively high. In contrast to the behaviour of the material of variant 3YSZ-1550, the XRD pattern of 4YSZ ceramics

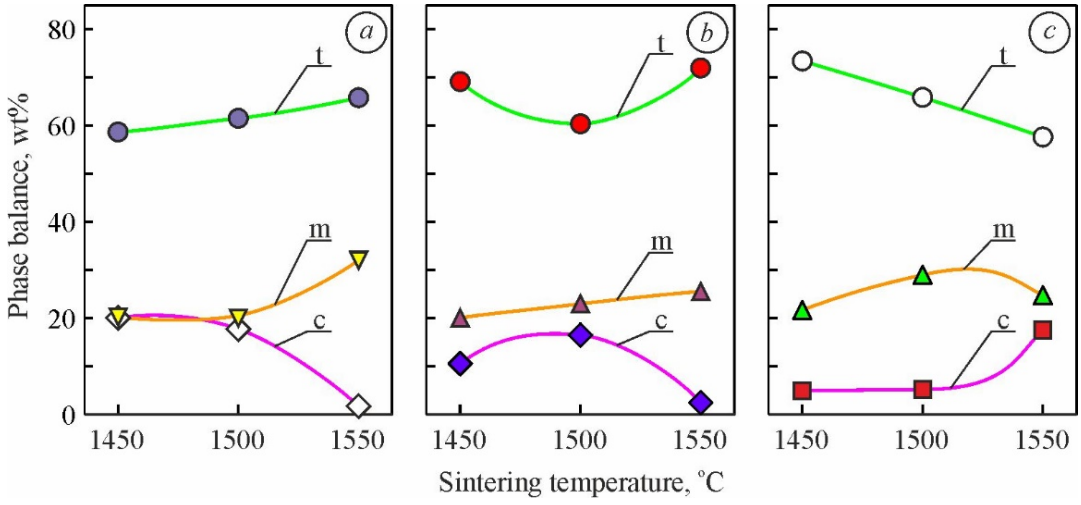

Fig. 1. Changes in zirconia phase balance of the investigated materials of variants (a) 3YSZ-1450, 3YSZ-1500, 3YSZ-1550, (b) 4YSZ-1450, 4YSZ-1500, 4YSZ-1550, and (c) 5YSZ-1450, 5YSZ-1500, 5YSZ-1550 depending on the sintering temperature (see Tab. 1). Phase marking: t – tetragonal, m – monoclinic, c – cubic

of variant 4YSZ-1500 exhibits a slightly different behaviour (Fig. 2b). Relatively lower peaks of the t-ZrO_2 and m-ZrO_2 phases, but much higher peaks of the c-ZrO_2 phase characterize this material. The XRD patterns of the material of variants 5YSZ-1450 and 5YSZ-1550 (Fig. 2c and Fig. 2d, respectively) display the general phase balance in 5YSZ ceramics, as they correspond to the extreme positions of the sintering temperature range of 1450-1550°C. However, the trend of changes in the phase balance with changes in the sintering temperature of this material from 1450°C to 1550°C is opposite to that found for the material of variants 3YSZ-1450, 3YSZ-1500, and 3YSZ-1550 (see Fig. 1a). The peaks of the t-ZrO_2 phase for the material of variant 5YSZ-1450 are of maximum height as compared to other studied variants (Fig. 2c), and for the material of variant 5YSZ-1550, they are much lower. The opposite behaviour is observed for the other two phases. That is, for the material of variant 5YSZ-1550, the peaks of the m-ZrO_2 phase and, in particular, of the c-ZrO_2 phase are significantly higher compared to the peaks for the material of variant 5YSZ-1450. The rapid growth of the peaks and, accordingly, the amount of cubic phase occurred due to its stabilization at a sintering temperature of 1550°C with a relatively large amount of yttria.

Thus, in 3YSZ and 4YSZ ceramics, the sintering temperature of 1550°C allows providing a relatively large amount of tetragonal phase of zirconia (over 65 wt.%), while the monoclinic phase is the balance because the amount of cubic phase is insignificant (up to 5 wt.%). In 5YSZ ceramics at this sintering temperature, the maximum amount of cubic phase for such a chemical composition was obtained, but the maximum amount of tetragonal phase of zirconia (over 73 wt.%) was obtained at a sintering temperature of 1450°C.

Therefore, the general tendencies of change of phase balance in yttria-stabilized zirconia are as follows: (i) with increasing sintering temperature the amount of tetragonal and monoclinic phases increases when the content of the

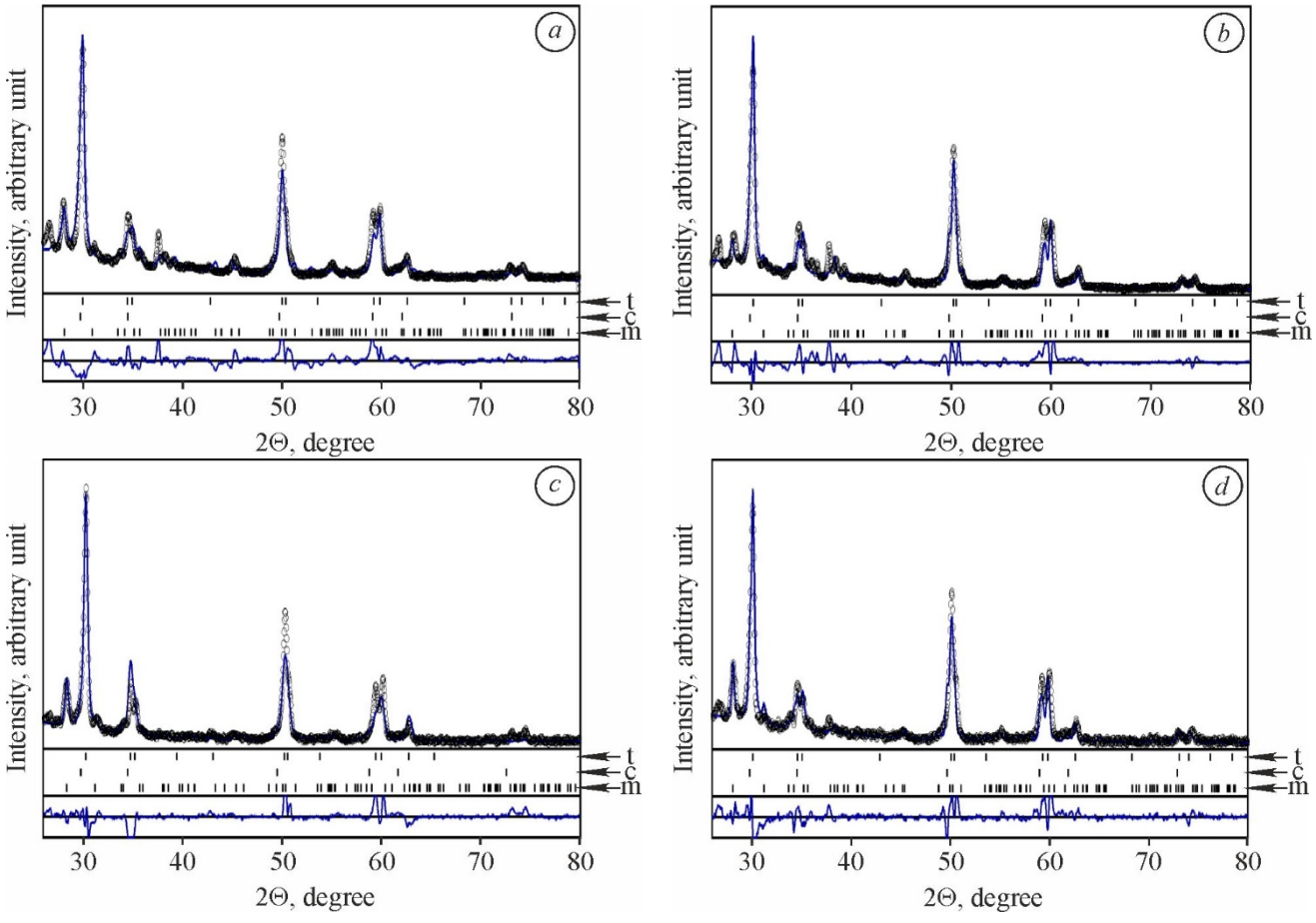

Fig. 2. XRD patterns of the investigated materials of variants (a) 3YSZ-1550, (b) 4YSZ-1500, (c) 5YSZ-1450, and (d) 5YSZ-1550 depending on the sintering temperature (see Tab. 1). Phase marking: t – tetragonal, m – monoclinic, c – cubic

stabilizing Y_2O_3 additive is insignificant; (ii) with increasing sintering temperature the amount of tetragonal and monoclinic phases decreases when the content of the stabilizing Y_2O_3 additive is relatively high. Therefore, to achieve a relatively high content of metastable tetragonal phase, zirconia with a low content of the stabilizing Y_2O_3 additive must be sintered at a temperature of 1550°C, and zirconia with a higher content of the additive must be sintered at 1450°C. Under these conditions, a minimum amount of cubic phase is formed.

3.2. Mechanical properties and the microstructural aspect

In the work [77], microhardness data set under the indentation loads of 0.49 N, 0.98 N, 1.96 N, 2.94 N, 4.91 N, and 9.81 N was obtained for yttria-stabilized zirconia (ZrO_2-8 mol% Y_2O_3) and a power function was fitted to the data. It was concluded that for the ceramics of this system there is a dependence of the material microhardness on the indentation load known as the indentation size effect [81-83] when the average values of microhardness decrease with increasing indentation load. However, at indentation loads ranged from 4.91 N to 9.81 N (the last value was the upper limit of a microhardness device), a tendency was observed with the yield of microhardness values on the plateau. The values of microhardness and fracture toughness obtained in this range of indentation loads are invariant.

According to the results of microhardness measurements of the studied material variants under the indentation loads of 0.49 N, 0.98 N, 1.96 N, 2.94 N, 4.91 N, and 9.81 N, the dependences were obtained (Fig. 3), of which 3YSZ-1550, 4YSZ-1450, 4YSZ-1550, 5YSZ-1450, and 5YSZ-1550 are characterized by decreasing the average values of microhardness with increasing indentation load.

In dependences 3YSZ-1450, 3YSZ-1500, 4YSZ-1500, and 5YSZ-1500, on the contrary, under the lowest load, the values of microhardness are minimal, which is not typical of ceramics, and the phase balance of these ceramics is characterized by the total maximum of cubic and monoclinic phases with the predominance of the latter one. However, for all the dependences, the yield of average values on the plateau at indentation loads from 4.91 N to 9.81 N was observed.

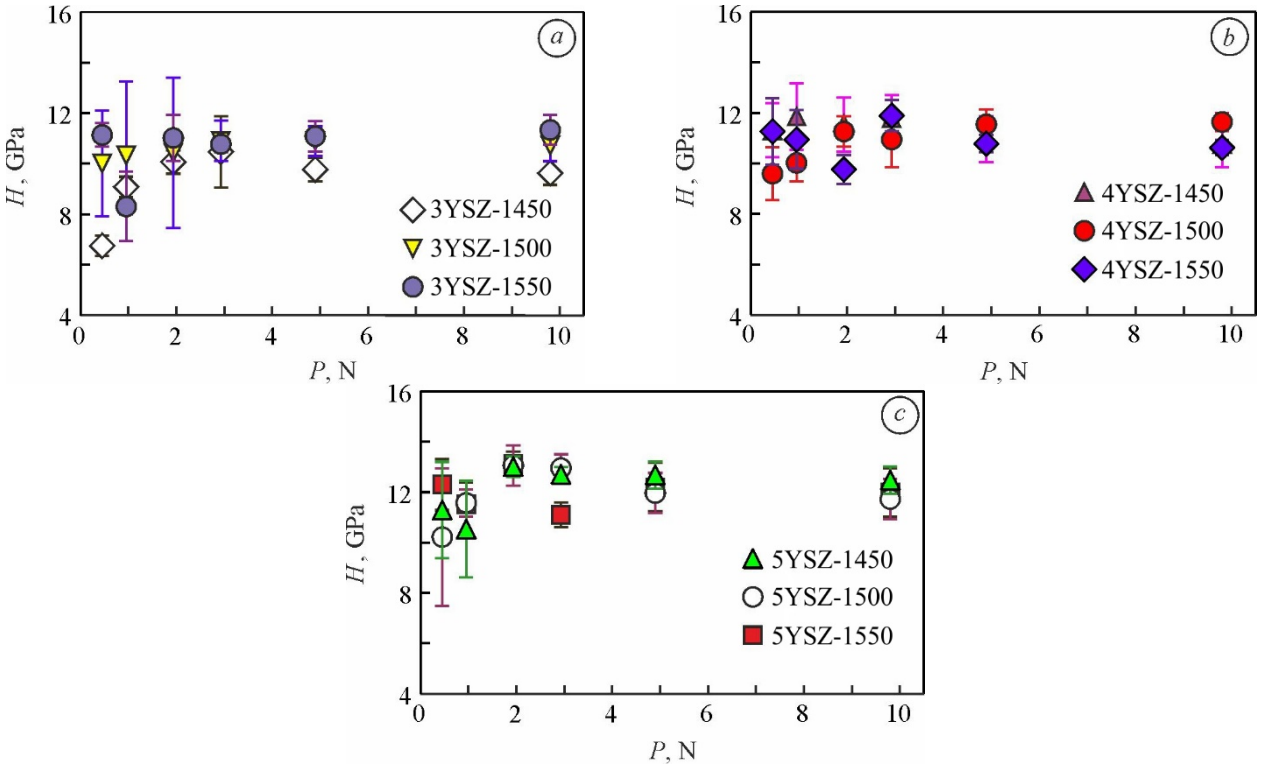

Fig. 3. The microhardness versus indentation load dependences for (a) 3YSZ, (b) 4YSZ, and (c) 5YSZ ceramics sintered at a temperature of 1450°C (variants 3YSZ-1450, 4YSZ-1450, and 5YSZ-1450), 1500°C (variants 3YSZ-1500, 4YSZ-1500, and 5YSZ-1500), and 1550°C (variants 3YSZ-1550, 4YSZ-1550, and 5YSZ-1550). The variant numbers (see Tab. 1) correspond to the symbol numbers

The invariant values of microhardness of the studied ceramic variants obtained under the indentation load of 9.81 N demonstrate the evolution of changes in the mechanical behaviour of the material with a change in the sintering temperature from 1450°C to 1550°C (Fig. 4).

The highest microhardness of 3YSZ ceramics was obtained at a sintering temperature of 1550°C (curve 3YSZ in Fig. 4). However, for 4YSZ ceramics, the sintering temperature of 1500°C (curve 4YSZ) is optimal, because the material obtained by this mode shows the highest microhardness compared to sintered at temperatures of 1450°C and 1550°C. 5YSZ ceramics sintered at 1500°C have the lowest microhardness, in contrast to 4YSZ ceramics, and the highest microhardness values are obtained for 5YSZ ceramics sintered at 1450°C. This ambiguity of the change in microhardness with the change in the sintering temperature of the material is due to the influence of an amount of the stabilizing additive and, as a consequence, the corresponding phase balance in the sintered materials (see Fig. 3). We observe a correlation between the phase percentage (Fig. 3) and microhardness of the studied material variants (Fig. 4).

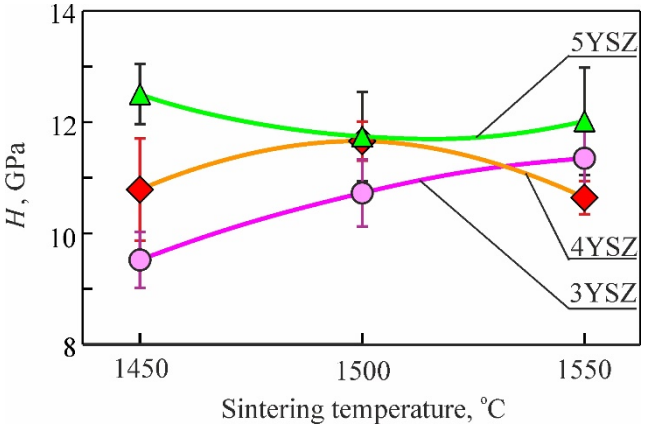

Fig. 4. Changes in microhardness of 3YSZ, 4YSZ, and 5YSZ ceramics depending on the sintering temperature (see Tab. 1). The measurements were performed under the indentation load of 9.81 N

To assess the fracture toughness of ceramics by the Vickers indentation method, the authors of several works [58, 59, 72] used the formula (2), which provided values close to those obtained by other methods of fracture mechanics. Therefore, we used this formula to estimate the crack growth resistance of the studied variants of YSZ ceramics. Thus, the values of the fracture toughness of the studied material variants were calculated by the formula (2) for each level of indentation load P and the corresponding value of microhardness H (see Fig. 3), using the approach proposed in the work [77].

Functions fitted to the corresponding experimental data of the materials under study (Fig. 5a) exhibit the behaviour of ceramic compositions similar to the trends in microhardness (Fig. 4). Besides, the fracture toughness dependences obtained using the SENB test method (Fig. 5b) also exhibit similar behaviour.

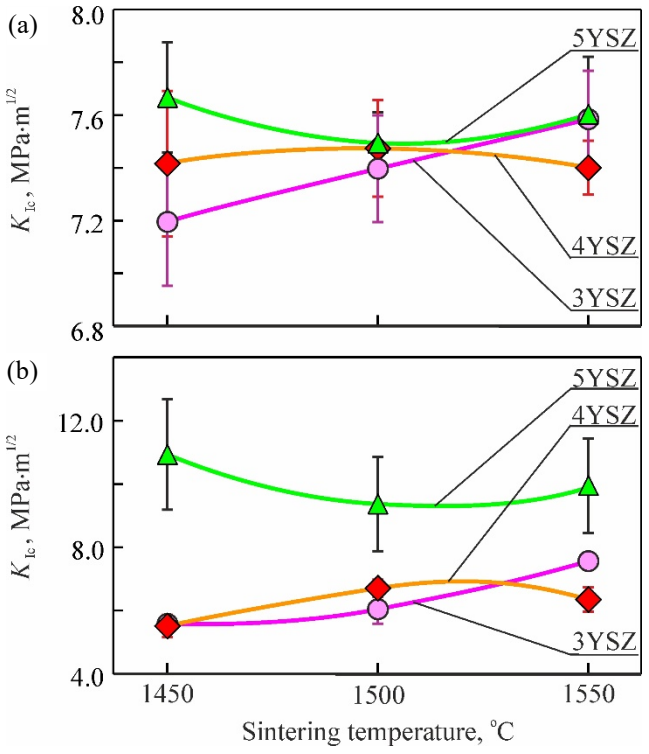

Fig. 5. Changes in fracture toughness of 3YSZ, 4YSZ, and 5YSZ ceramics depending on the sintering temperature (see Tab. 1): a) Vickers indentation method under the indentation load of 9.81 N; b) SENB method under three-point bending

For 5YSZ ceramics, we can see a minimum on the corresponding curve close to the sintering temperature of 1500°C, whereas for 3YSZ and 4YSZ ceramics no unambiguous tendency is observed since the character of the curves differs depending on the type of fracture toughness test (SENB test or Vickers indentation test). This ambiguous behaviour evidences that the sintering temperature of the material, slightly above 1500°C, is critical in the microstructure formation process.

Thus, for 3YSZ, 4YSZ, and 5YSZ ceramics, phase balances are defined at which the maximum fracture toughness is reached. Such material variants are

characterized by the distinct microstructure (Fig. 6) and morphology of the fracture surface (Fig. 7). Thus, the maximum fracture toughness of 3YSZ ceramics is reached at the maximum content of the tetragonal phase (variant 3YSZ-1550). In the picture of the SEM microstructure of such a specimen (Fig. 6a), agglomerates uniformly distributed in the matrix of t-ZrO_2 are observed. These agglomerates consist of particles of about 2-4 μm in size. No clear contours of the tetragonal phase particles are seen. However, it seems that the average particle size is less than 1 μm since in the picture of SEM fracture surface of such a specimen (Fig. 7a), a distinct intergranular fracture micromechanism is observed and separate grains are less than 1 μm in size.

In 5YSZ ceramics of variant 5YSZ-1450, it is already possible to distinguish blurred contours of nano-agglomerates of the t-ZrO_2 phase of about 200-250 nm in size (Fig. 6c). The fracture along the boundaries of such nanograins occurs during the fracture toughness test (Fig. 7c) exhibiting a distinct intergranular fracture micromechanism. This material has the highest fracture toughness among the studied ones (see Fig. 5) which correlates with an amount of the t-ZrO_2 phase (see Fig. 1c).

In 5YSZ ceramics of variant 5YSZ-1550, we can observe, in contrast to the ceramics of variant 5YSZ-1450, some ordering of the former t-ZrO_2 phase agglomerates (Fig. 6d) which can evidence the presence of some quantity of the c-ZrO_2 phase. Such c-ZrO_2 phase nanoparticles are

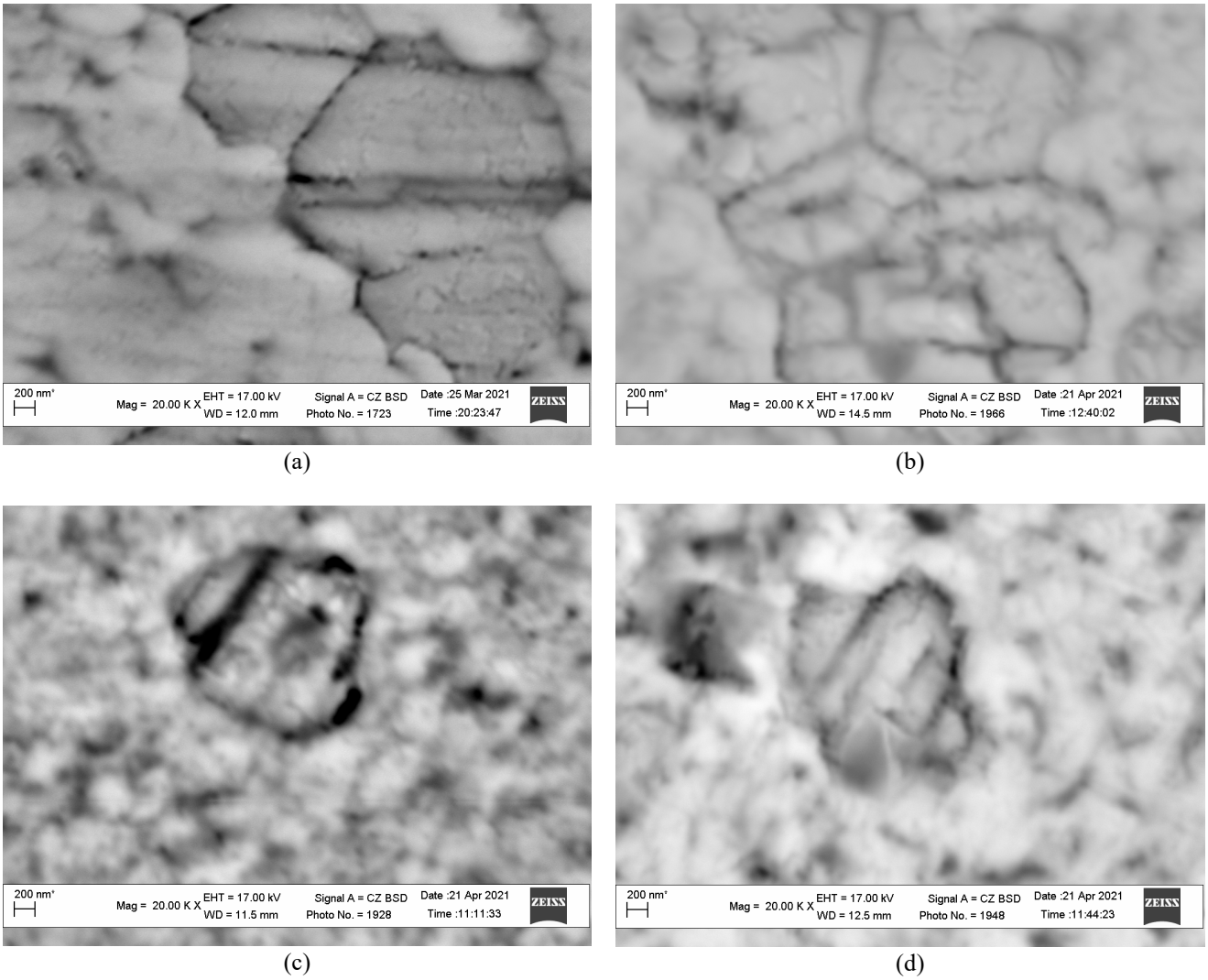

Fig. 6. SEM microstructures (BSD images) of specimens of (a) 3YSZ ceramics sintered at 1550°C, (b) 4YSZ ceramics sintered at 1500°C, (c) 5YSZ ceramics sintered at 1450°C, and (d) 5YSZ ceramics sintered at 1550°C

observed on the fracture surface of the specimen (Fig. 7d). These particles are located along the boundaries of t-ZrO_2 phase grains, the size of which is close to that of grains in material variant 3YSZ-1550. Probably, such coarsening of t-ZrO_2 phase grains is a result of enhanced sintering temperature causing intense grain growth. Despite some amount of the c-ZrO_2 phase, fracture toughness of this material is lower than of the material variant 5YSZ-1450 that probably is a result of a lower amount of the t-ZrO_2 phase (see Fig. 1c).

A sintering temperature of 1500°C is the most appropriate for 4YSZ ceramics (variant 4YSZ-1500). This material, having fracture toughness lower than the material variant 3YSZ-1550, was formed due to the competing action of the sintering temperature of the ceramics and the content of the stabilizing Y_2O_3 additive. As a result of such the competition, the corresponding microstructure was formed (Fig. 6b), and a lower amount of the t-ZrO_2 phase as compared to two other variants (4YSZ-1450 and 4YSZ-1550) of 4YSZ ceramics was reached (see Fig. 1b). Despite a quite high amount of the c-ZrO_2 phase, it does not contribute noticeably to the fracture toughness level of this material. Fragmentation of course particles of the m-ZrO_2 phase (Fig. 6b) is followed by cleavage along the boundaries of such subgrains in combination with intergranular crack growth along the boundaries of the t-ZrO_2 phase (Fig. 7b).

Thus, in terms of mechanical behaviour, the best variant of material is that of 5YSZ ceramics sintered at a temperature of 1450°C (variant 5YSZ-1450).

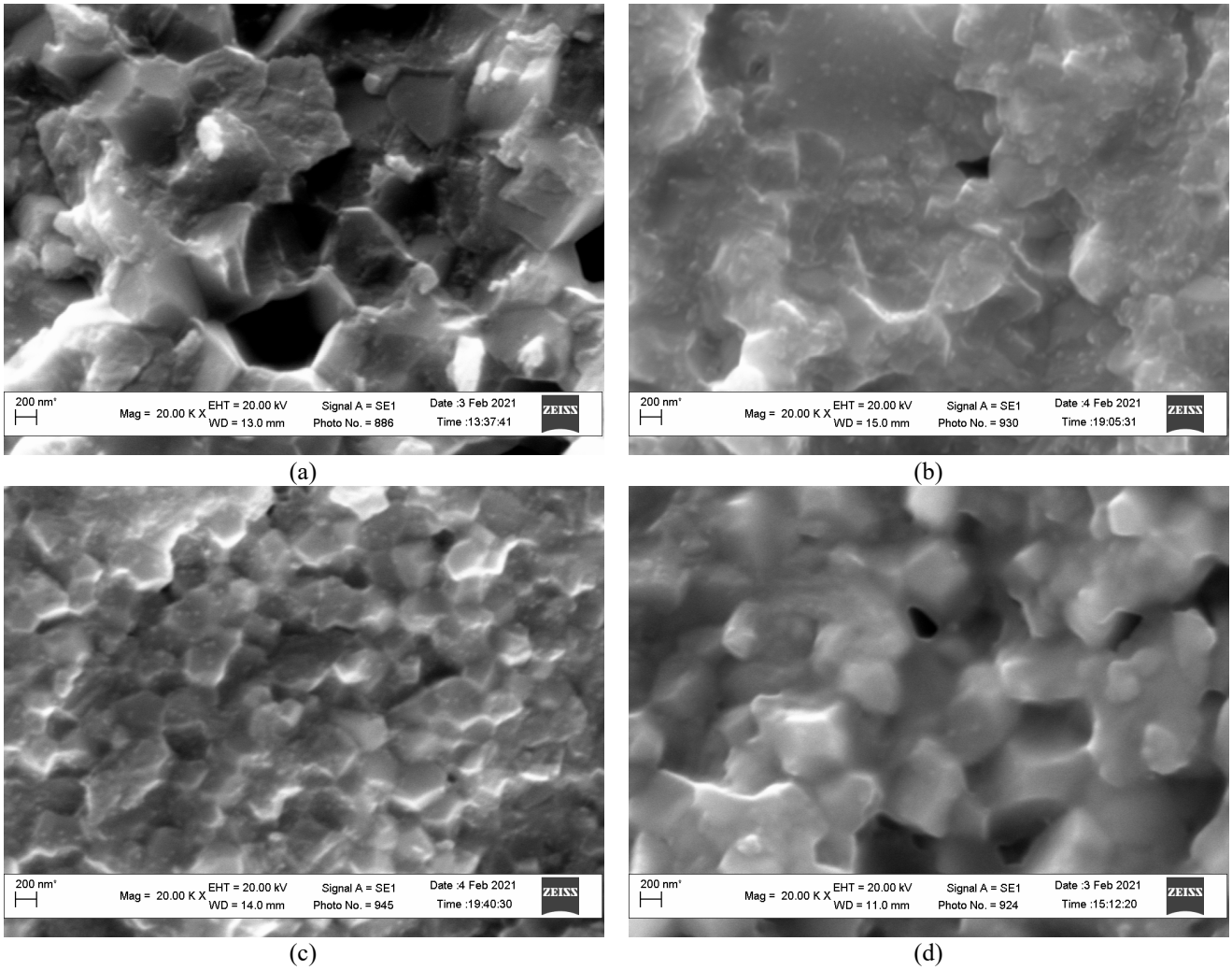

Fig. 7. SEM fractography (SE images) of specimens of (a) 3YSZ ceramics sintered at 1550°C, (b) 4YSZ ceramics sintered at 1500°C, (c) 5YSZ ceramics sintered at 1450°C, and (d) 5YSZ ceramics sintered at 1550°C

4. Conclusions

1. In this work, the microstructure and physical and mechanical properties of 3YSZ, 4YSZ, and 5YSZ ceramics have been studied. It was shown that the fracture toughness of YSZ material is a characteristic sensitive to microstructural changes occurring in the material due to phase transformations in the presence of a stabilizing additive in the investigated sintering temperature range.
2. For each of the studied modes of sintering YSZ ceramics, the conditions for the formation of tetragonal, monoclinic, and cubic phases of zirconia in corresponding material modifications were substantiated.
3. In 5YSZ ceramics sintered at a temperature of 1450°C, the highest level of fracture toughness was reached as compared to those of other studied material variants. The fracture toughness of this material correlates with a high percentage of the tetragonal phase of zirconia.

Acknowledgements

The authors are deeply grateful to the staff of the Center of Electron Microscopy and X-ray Diffraction Microanalysis at Karpenko Physico-Mechanical Institute of the National Academy of Sciences of Ukraine (headed by Prof. V. I. Pokhmurs'kyi) for their kind help in performing the microstructural and microfractographic studies.

References

[1] M. Spyrka, R. Atraszkiewicz, L. Klimek, A new ceramic composite based on spherical aluminium oxide for auxiliary panels in high-temperature firing processes, Archives of Materials Science and Engineering 101/1 (2020), 5-14. DOI: https://doi.org/10.5604/01.3001.0013.9501

[2] L.A. Dobrzański, L.B. Dobrzański, A.D. Dobrzańska-Danikiewicz, Manufacturing technologies thick-layer coatings on various substrates and manufacturing gradient materials using powders of metals, their alloys and ceramics, Journal of Achievements in Materials and Manufacturing Engineering 99/1 (2020) 14-41. DOI: https://doi.org/10.5604/01.3001.0014.1598

[3] Ye. Kharchenko, Z. Blikharskyy, V. Vira, B.D. Vasyliv, V.Ya. Podhurska, A. Kalynovskyy, V. Korendiy, Nanostructural changes in a Ni/NiO cermet during high-temperature reduction and reoxidation, in: O. Fesenko, L. Yatsenko (eds.), Nanomaterials and Nanocomposites, Nanostructure Surfaces, and Their Applications, Springer Proceedings in Physics, vol. 246, Springer, Cham. 2021, 219-229. DOI: https://doi.org/10.1007/978-3-030-51905-6_17

[4] L.Ya. Ropyak, M.V. Makoviichuk, I.P. Shatskyi, I.M. Pritula, L.O. Gryn, V.O. Belyakovskyi, Stressed state of laminated interference-absorption filter under local loading, Functional Materials 27/3 (2020) 638-642. DOI: https://doi.org/10.15407/fm27.03.638

[5] V.M. Posuvailo, V.V. Kulyk, Z.A. Duriagina, I.V. Koval'chuck, M.M. Student, B.D. Vasyliv, The effect of electrolyte composition on the plasma electrolyte oxidation and phase composition of oxide ceramic coatings formed on 2024 aluminium alloy, Archives of Materials Science and Engineering 105/2 (2020) 49-55. DOI: https://doi.org/10.5604/01.3001.0014.5761

[6] T.S. Cherepova, H.P. Dmytrieva, O.I. Dukhota, M.V. Kindrachuk, Properties of nickel powder alloys hardened with titanium carbide, Materials Science 52/2 (2016) 173-179. DOI: https://doi.org/10.1007/s11003-016-9940-2

[7] S.S. Savka, D.I. Popovych, A.S. Serednytski, Molecular dynamics simulations of the formation processes of zinc oxide nanoclusters in oxygen environment, in: O. Fesenko, L. Yatsenko (eds.), Nanophysics, Nanomaterials, Interface Studies, and Applications. NANO 2016. Springer Proceedings in Physics, vol. 195, Springer, Cham, 2017, 145-156. DOI: https://doi.org/10.1007/978-3-319-56422-7_11

[8] L.A. Dobrzański, L.B. Dobrzański, A.D. Dobrzańska-Danikiewicz, Overview of conventional technologies using the powders of metals, their alloys and ceramics in Industry 4.0 stage, Journal of Achievements in Materials and Manufacturing Engineering 98/2 (2020) 56-85. DOI: https://doi.org/10.5604/01.3001.0014.1481

[9] J. Milewski, J. Kupecki, A. Szczęśniak, N. Uzunow, Hydrogen production in solid oxide electrolyzers coupled with nuclear reactors, International Journal of Hydrogen Energy (2020) (available online). DOI: https://doi.org/10.1016/j.ijhydene.2020.11.217

[10] D.R. Clarke, C.G. Levi, Material design for the next generation thermal barrier coatings, Annual Review of Materials Research 33/1 (2003) 383-417. DOI: https://doi.org/10.1146/annurev.matsci.33.011403.113718

[11] B. Vasyliv, V. Podhurska, O. Ostash, Preconditioning of the YSZ-NiO fuel cell anode in hydrogenous atmospheres containing water vapor, Nanoscale

Research Letters 12 (2017) 265. DOI: https://doi.org/10.1186/s11671-017-2038-4

[12] M. Szota, A. Łukaszewicz, K. Machnik, The possibility to control the thickness of the oxide layer on the titanium Grade 2 by mechanical activation and heat treatment, Journal of Achievements in Materials and Manufacturing Engineering 100/2 (2020) 70-77. DOI: https://doi.org/10.5604/01.3001.0014.3346

[13] G. Witz, V. Shklover, W. Steurer, S. Bachegowda, H.-P. Bossmann, Phase evolution in yttria-stabilized zirconia thermal barrier coatings studied by Rietveld refinement of X-ray powder diffraction patterns, Journal of the American Ceramic Society 90/9 (2007) 2935-2940. DOI: https://doi.org/10.1111/j.1551-2916.2007.01785.x

[14] K. Buła, A. Palatyńska-Ulatowska, L. Klimek, Biodentine management and setting time with Vicat and Vickers evaluation; a survey-based study on clinicians' experience, Archives of Materials Science and Engineering 103/2 (2020) 75-85. DOI: https://doi.org/10.5604/01.3001.0014.3358

[15] X.W. Zhou, Y.F. Shen, H.M. Jin, Effect of deposition mechanism and microstructure of nano-ceria oxide addition on Ni-P coating by pulse electrodeposition, Advanced Materials Research 326 (2011) 151-156. https://doi.org/10.4028/www.scientific.net/AMR.326.151

[16] B. Vasyliv, J. Milewski, V. Podhurska, T. Wejrzanowski, V. Kulyk, J. Skibiński, V. Vira, Ł. Szabłowski, A. Szczęśniak, O. Dybiński, Study of the degradation of a fine-grained YSZ-NiO anode material during reduction in hydrogen and reoxidation in air, Applied Nanoscience (2021).
DOI: https://doi.org/10.1007/s13204-021-01768-w

[17] O.V. Sukhova, Influence of mechanisms of structure formation of interfaces in composites on their properties, Metallofizika i Noveishie Tekhnologii 31/7 (2009) 1001-1012.

[18] V.G. Efremenko, Yu.G. Chabak, K. Shimizu, A.G. Lekatou, V.I. Zurnadzhy, A.E. Karantzalis, H. Halfa, V.A. Mazur, B.V. Efremenko, Structure refinement of high-Cr cast iron by plasma surface melting and post-heat treatment, Materials and Design 126 (2017) 278-290.
DOI: https://doi.org/10.1016/j.matdes.2017.04.022

[19] M. Kujawa, R. Suwak, L.A. Dobrzański, A. Gerle, B. Tomiczek, Thermal characterization of halloysite materials for porous ceramic preforms, Archives of Materials Science and Engineering 107/1 (2021) 5-15. DOI: https://doi.org/10.5604/01.3001.0014.8189

[20] I.B. Ivasenko, V.M. Posuvailo, M.D. Klapkiv, V.A. Vynar, S.I. Ostap'yuk, Express method for determining the presence of defects of the surface of oxide-ceramic coatings, Materials Science 45/3 (2009) 460-464. DOI: https://doi.org/10.1007/s11003-009-9191-6

[21] R.A. Miller, J.L. Smialek, R.G. Garlick, Phase stability in plasma sprayed, partially stabilized zirconia-yttria, in: A.H. Heuer, L.W. Hobbs (eds.), Advances in Ceramics, Vol. 3, Science and Technology of Zirconia I, American Ceramic Society, Columbus, 1981, 241-253.

[22] J. Ilavsky, J.K. Stalick, J. Wallace, Thermal spray yttria-stabilized zirconia phase changes during annealing, Journal of Thermal Spray Technology 10/3 (2001) 497-501.
DOI: https://doi.org/10.1361/105996301770349277

[23] J.R. Brandon, R. Taylor, Phase stability of zirconia-based thermal barrier coatings Part I, Zirconia-yttria alloys, Surface and Coatings Technology 46/1 (1991) 75-90.
DOI: https://doi.org/10.1016/0257-8972(91)90151-L

[24] U. Schulz, Phase transformation in EB-PVD yttria partially stabilized zirconia thermal barrier coatings during annealing, Journal of the American Ceramic Society 83/4 (2000) 904-910. DOI: https://doi.org/10.1111/j.1151-2916.2000.tb01292.x

[25] A. Azzopardi, R. Mevrel, B. Saint-Ramond, E. Olson, K. Stiller, Influence of aging on structure and thermal conductivity of Y-PSZ and Y-FSZ EB-PVD coatings, Surface and Coatings Technology 177-178 (2004) 131-139.
DOI: https://doi.org/10.1016/j.surfcoat.2003.08.073

[26] J. Katamura, T. Sakuma, Computer simulation of the microstructural evolution during the diffusionless cubic-to-tetragonal transition in the system ZrO_2–Y_2O_3, Acta Materialia 46/5 (1998) 1569-1575. DOI: https://doi.org/10.1016/S1359-6454(97)00356-X

[27] H.G. Scott, Phase relationships in the zirconia-yttria system, Journal of Materials Science 10 (1975) 1527-1535. DOI: https://doi.org/10.1007/BF01031853

[28] F. Kern, A. Gommeringer. Mechanical properties of 2Y-TZP fabricated from detonation synthesized powder, Ceramics 3/4 (2020) 440-452. DOI: https://doi.org/10.3390/ceramics3040037

[29] A. Kumar, P. Kumar, A.S. Dhaliwal, Structural studies of zirconia and yttria doped zirconia for analysing it phase stabilization criteria, IOP Conference Series: Materials Science and Engineering 1033 (2021) 012052. DOI: https://doi.org/10.1088/1757-899X/1033/1/012052

[30] M.F.R.P. Alves, S. Ribeiro, P.A. Suzuki, K. Strecker, C. dos Santos, Effect of Fe_2O_3 addition and sintering temperature on mechanical properties and translucence

of zirconia dental ceramics with different Y_2O_3 content, Materials Research 24/2 (2021) e20200402. DOI: https://doi.org/10.1590/1980-5373-MR-2020-0402

[31] K.-W. Jeong, J.-S. Han, G.-U. Yang, D.-J. Kim, Influence of preaging temperature on the indentation strength of 3Y-TZP aged in ambient atmosphere, Materials 14 (2021) 2767. DOI: https://doi.org/10.3390/ma14112767

[32] Y.-Y. Tsai, T.-M. Lee, J.-C. Kuo, Hydrothermal-aging-induced lattice distortion in yttria-stabilized zirconia using EBSD technique, Micron 145 (2021) 103053. DOI: https://doi.org/10.1016/j.micron.2021.103053

[33] S.H. Ji, D.S. Kim, M.S. Park, J.S. Yun, Sintering process optimization for 3YSZ ceramic 3D-printed objects manufactured by stereolithography, Nanomaterials 11/1 (2021) 192. DOI: https://doi.org/10.3390/nano11010192

[34] A. Gaddam, D.S. Brazete, A.S. Neto, B. Nan, J.M.F. Ferreira, Three-dimensional printing of zirconia scaffolds for load bearing applications: Study of the optimal fabrication conditions, Journal of the American Ceramic Society 104/9 (2021) 4368-4380. DOI: https://doi.org/10.1111/jace.17874

[35] S. Tao, J. Yang, M. Zhai, F. Shao, X. Zhong, H. Zhao, Y. Zhuang, J. Ni, W. Li, S. Tao, Thermal stability of YSZ thick thermal barrier coatings deposited by suspension and atmospheric plasma spraying, Crystals 10/11 (2020) 984. DOI: https://doi.org/10.3390/cryst10110984

[36] M. Rudolphi, M.C. Galetz, M. Schütze, Mechanical stability diagrams for thermal barrier coating systems, Journal of Thermal Spray Technology 30 (2021) 694-707. DOI: https://doi.org/10.1007/s11666-021-01163-5

[37] Z. Fan, X. Sun, X. Zhuo, X. Mei, J. Cui, W. Duan, W. Wang, X. Zhang, L. Yang, Femtosecond laser polishing yttria-stabilized zirconia coatings for improving molten salts corrosion resistance, Corrosion Science 184 (2021) 109367. DOI: https://doi.org/10.1016/j.corsci.2021.109367

[38] L.A. Dobrzański, L.B. Dobrzański, A.D. Dobrzańska-Danikiewicz, Additive and hybrid technologies for products manufacturing using powders of metals, their alloys and ceramics, Archives of Materials Science and Engineering 102/2 (2020) 59-85. DOI: https://doi.org/10.5604/01.3001.0014.1525

[39] I.M. Andreiko, V.V. Kulyk, O.P. Ostash, Resistance of steels of railroad wheels to corrosion-fatigue fracture, Materials Science 47/5 (2012) 608-612. DOI: https://doi.org/10.1007/s11003-012-9434-9

[40] A. Sciazko, T. Shimura, Y. Komatsu, N. Shikazono, Ni-GDC and Ni-YSZ electrodes operated in solid oxide electrolysis and fuel cell modes, Journal of Thermal Science and Technology 16/1 (2021) JTST0013. DOI: https://doi.org/10.1299/jtst.2021jtst0013

[41] V.G. Efremenko, Yu.G. Chabak, A. Lekatou, A.E. Karantzalis, A.V. Efremenko, High-temperature oxidation and decarburization of 14.55 wt. pct Cr-cast iron in dry air atmosphere, Metallurgical and Materials Transactions A 47/2 (2016) 1529-1543. DOI: https://doi.org/10.1007/s11661-016-3336-7

[42] H. Nykyforchyn, H. Krechkovska, O. Student, O. Zvirko, Feature of stress corrosion cracking of degraded gas pipeline steels, Procedia Structural Integrity 16 (2019) 153-160. DOI: https://doi.org/10.1016/j.prostr.2019.07.035

[43] O.M. Romaniv, B.D. Vasyliv, Some features of formation of the structural strength of ceramic materials, Materials Science 34/2 (1998) 149-161. DOI: https://doi.org/10.1007/BF02355530

[44] A. Włodarczyk-Fligier, M. Polok-Rubiniec, J. Konieczny, Thermal analysis of matrix composite reinforced with Al_2O_3 particles, Journal of Achievements in Materials and Manufacturing Engineering 100/1 (2020) 5-11. DOI: https://doi.org/10.5604/01.3001.0014.1957

[45] S. Buchaniec, A. Sciazko, M. Mozdzierz, G. Brus, A novel approach to the optimization of a solid oxide fuel cell anode using evolutionary algorithms, IEEE Access 7 (2019) 34361-34372. DOI: https://doi.org/10.1109/ACCESS.2019.2904327

[46] O.M. Romaniv, I.V. Zalite, V.M Simin'kovych, O.N. Tkach, B.D. Vasyliv, Effect of the concentration of zirconium dioxide on the fracture resistance of Al_2O_3–ZrO_2 ceramics, Materials Science 31/5 (1996) 588-594. DOI: https://doi.org/10.1007/BF00558793

[47] A.S. Buyakov, Yu.A. Mirovoy, A.Yu. Smolin, S.P. Buyakova, Increasing fracture toughness of zirconia-based composites as a synergistic effect of the introducing different inclusions, Ceramics International 47/8 (2021) 10582-10589. DOI: https://doi.org/10.1016/j.ceramint.2020.12.170

[48] P. Khajavi, P.V. Hendriksen, J. Chevalier, L. Gremillard, H.L. Frandsen, Improving the fracture toughness of stabilized zirconia-based solid oxide cells fuel electrode supports: Effects of type and concentration of stabilizer(s), Journal of the European Ceramic Society 40/15 (2020) 5670-5682. DOI: https://doi.org/10.1016/j.jeurceramsoc.2020.05.042

[49] A.D. Ivasyshyn, B.D. Vasyliv, Effect of the size and form of specimens on the diagram of growth rates of fatigue cracks, Materials Science 37/6 (2001) 1002-1004. DOI: https://doi.org/10.1023/A:1015669913601

[50] B.D. Vasyliv, Initiation of a crack from the edge of a notch with oblique front in specimens of brittle materials, Materials Science 38/5 (2002) 724-728. DOI: https://doi.org/10.1023/A:1024222709514
[51] Y. Komatsu, A. Sciazko, N. Shikazono, Isostatic pressing of screen printed nickel-gadolinium doped ceria anodes on electrolyte-supported solid oxide fuel cells, Journal of Power Sources 485 (2021) 229317. DOI: https://doi.org/10.1016/j.jpowsour.2020.229317
[52] B.D. Vasyliv, Improvement of the electric conductivity of the material of anode in a fuel cell by the cyclic redox thermal treatment, Materials Science 46/2 (2010) 260-264. DOI: https://doi.org/10.1007/s11003-010-9282-4
[53] I. Danilenko, G. Lasko, I. Brykhanova, V. Burkhovetski, L. Ahkhozov, The peculiarities of structure formation and properties of zirconia-based nanocomposites with addition of Al_2O_3 and NiO, Nanoscale Research Letters 12 (2017) 125. DOI: https://doi.org/10.1186/s11671-017-1901-7
[54] V. Podhurska, B. Vasyliv, Influence of NiO reduction on microstructure and properties of porous Ni–ZrO_2 substrates, Proceedings of the 2012 IEEE International Conference on Oxide Materials for Electronic Engineering "OMEE", Lviv, 2012, 293-294. DOI: https://doi.org/10.1109/OMEE.2012.6464761
[55] ASTM E 384-11. Standard test method for Knoop and Vickers hardness of materials, ASTM International, 2011. DOI: https://doi.org/10.1520/E0384-11
[56] ASTM C 1327-03. Standard test method for Vickers indentation hardness of advanced ceramics, ASTM International, 2003. DOI: https://doi.org/10.1520/C1327-03
[57] O.P. Ostash, V.V. Kulyk, T.M. Lenkovskiy, Z.A. Duriagina, V.V. Vira, T.L. Tepla, Relationships between the fatigue crack growth resistance characteristics of a steel and the tread surface damage of railway wheel, Archives of Materials Science and Engineering 90/2 (2018) 49-55. DOI: https://doi.org/10.5604/01.3001.0012.0662
[58] R.F. Cook, G.M. Pharr, Direct observation and analysis of indentation cracking in glasses and ceramics, Journal of the American Ceramic Society, 73/4 (1990) 787-817. DOI: https://doi.org/10.1111/j.1151-2916.1990.tb05119.x
[59] A. Nastic, A. Merati, M. Bielawski, M. Bolduc, O. Fakolujo, M. Nganbe, Instrumented and Vickers indentation for the characterization of stiffness, hardness and toughness of zirconia toughened Al_2O_3 and SiC armor, Journal of Materials Science and Technology 31/8 (2015) 773-783. DOI: https://doi.org/10.1016/j.jmst.2015.06.005
[60] J.W. Adams, R. Ruh, K.S. Mazdiyasni, Young's modulus, flexural strength, and fracture of yttria-stabilized zirconia versus temperature, Journal of the American Ceramic Society 80/4 (1997) 903-908. DOI: https://doi.org/10.1111/j.1151-2916.1997.tb02920.x
[61] H.A. Shabri, M.H.D. Othman, M.A. Mohamed, T.A. Kurniawan, S.M. Jamil, Recent progress in metal-ceramic anode of solid oxide fuel cell for direct hydrocarbon fuel utilization: A review, Fuel Processing Technology 212 (2021) 106626. DOI: https://doi.org/10.1016/j.fuproc.2020.106626
[62] B.R. Lawn, Fracture of brittle solids, Second Edition, Cambridge University Press, Cambridge, 1993. DOI: https://doi.org/10.1017/CBO9780511623127
[63] B.R. Lawn, M.V. Swain, Microfracture beneath point indentations in brittle solids, Journal of Materials Science 10/1 (1975) 113-122. DOI: https://doi.org/10.1007/BF00541038
[64] B.R. Lawn, E.R. Fuller, Equilibrium penny-like cracks in indentation fracture, Journal of Materials Science 10/12 (1975) 2016-2024. DOI: https://doi.org/10.1007/BF00557479
[65] A.G. Evans, E.A. Charles, Fracture toughness determinations by indentation, Journal of the American Ceramic Society 59/7-8 (1976) 371-372. DOI: https://doi.org/10.1111/j.1151-2916.1976.tb10991.x
[66] K. Tanaka, Elastic/plastic indentation hardness and indentation fracture toughness: The inclusion core model, Journal of Materials Science 22/4 (1987) 1501-1508. DOI: https://doi.org/10.1007/BF01233154
[67] K. Niihara, R. Morena, D.P.H. Hasselman, Evaluation of K_{Ic} of brittle solids by the indentation method with low crack-to-indent ratios, Journal of Materials Science Letters 1/1 (1982) 13-16. DOI: https://doi.org/10.1007/BF00724706
[68] K. Niihara, A fracture mechanics analysis of indentation-induced Palmqvist crack in ceramics, Journal of Materials Science Letters 2/5 (1983) 221-223. DOI: https://doi.org/10.1007/BF00725625
[69] I. Danilenko, F. Glazunov, T. Konstantinova, I. Yashchyshyn, V. Burkhovetski, G. Volkova, Effect of Ni/NiO particles on structure and crack propagation in zirconia based composites, Advanced Materials Letters 5/8 (2014) 465-471. DOI: https://doi.org/10.5185/amlett.2014.amwc1040II
[70] O.N. Grigoriev, V.B. Vinokurov, T.V. Mosina, L.M. Melakh, N.D. Bega, A.V. Koroteev, L.I. Klimenko, A.V. Stepanenko, Kinetics of shrinkage, structurization, and the mechanical characteristics of zirconium boride sintered in the presence of activating additives, Powder Metallurgy and Metal

Ceramics 55/11-12 (2017) 676-688. DOI: https://doi.org/10.1007/s11106-017-9855-y
[71] G.A. Gogotsi, S.N. Dub, E.E. Lomonova, B.I. Ozersky, Vickers and Knoop indentation behaviour of cubic and partially stabilized zirconia crystals, Journal of the European Ceramic Society 15/5 (1995) 405-413. DOI: https://doi.org/10.1016/0955-2219(95)91431-M
[72] M.A. Aswad, Comparison of the fracture toughness of high temperature ceramic measured by digital image correlation and indentation method, Journal of University of Babylon 22/4 (2014) 927-937. Available at: https://www.iasj.net/iasj?func=article&aId=99010
[73] G.R. Anstis, P. Chantikul, B.R. Lawn, D.B. Marshall, A critical evaluation of indentation techniques for measuring fracture toughness: I, Direct crack measurement, Journal of the American Ceramic Society 64/9 (1981) 533-538. DOI: https://doi.org/10.1111/j.1151-2916.1981.tb10320.x
[74] B.R. Lawn, A.G. Evans, D.B. Marshall, Elastic/plastic indentation damage in ceramics: The median/radial crack system, Journal of the American Ceramic Society 63/9-10 (1980) 574-581. DOI: https://doi.org/10.1111/j.1151-2916.1980.tb10768.x
[75] J.E. Blendell, The origins of internal stresses in polycrystalline alumina and their effects on mechanical properties, Cambridge University Press, Cambridge, 1979.
[76] J. Lankford, Indentation microfracture in the Palmqvist crack regime: implications for fracture toughness evaluation by the indentation method, Journal of Materials Science Letters 1/11 (1982) 493-495. DOI: https://doi.org/10.1007/BF00721938
[77] B. Vasyliv, V. Kulyk, Z. Duriagina, D. Mierzwinski, T. Kovbasiuk, T. Tepla, Estimation of the effect of redox treatment on microstructure and tendency to brittle fracture of anode materials of YSZ-NiO(Ni) system, Eastern-European Journal of Enterprise Technologies 6/12(108) (2020) 67-77. DOI: https://doi.org/10.15587/1729-4061.2020.218291
[78] ASTM E 399-20A. Standard test method for linear-elastic plane-strain fracture toughness of metallic materials, ASTM International, 2020. DOI: https://doi.org/10.1520/E0399-20A
[79] ASTM C 1421-18. Standard test methods for determination of fracture toughness of advanced ceramics at ambient temperature, ASTM International, 2018. DOI: https://doi.org/10.1520/C1421-18
[80] J. Kübier, Fracture toughness of ceramics using the SEVNB method: From a preliminary study to a standard test method, in: J. Salem, G. Quinn, M. Jenkins (eds.), Fracture Resistance Testing of Monolithic and Composite Brittle Materials, ASTM International, West Conshohocken, 2002, 93-106. DOI: https://doi.org/10.1520/STP10473S
[81] Z. Peng, J. Gong, H. Miao, On the description of indentation size effect in hardness testing for ceramics: Analysis of the nanoindentation data, Journal of the European Ceramic Society 24/8 (2004) 2193-2201. DOI: https://doi.org/10.1016/S0955-2219(03)00641-1
[82] I.M. Spiridonova, E.V. Sukhovaya, S.B. Pilyaeva, O.G. Bezrukavaya, The use of composite coatings during metallurgical equipment parts repair, Metallurgicheskaya i Gornorudnaya Promyshlennost 3 (2002) 58-61.
[83] L.Ya. Ropyak, I.P. Shatskyi, M.V. Makoviichuk, Influence of the oxide-layer thickness on the ceramic-aluminium coating resistance to indentation, Metallofizika i Noveishie Tekhnologii 39/4 (2017) 517-524. DOI: https://doi.org/10.15407/mfint.39.04.0517